Solid Freeform Fabrication 2023: Proceedings of the 34th Annual International Solid Freeform Fabrication Symposium – An Additive Manufacturing Conference
Reviewed Paper

Comparison of process control methods for wire-arc directed energy deposition of low carbon steels with in-situ temperature measurement

Ahamed Ameen[1,2], Vit Janik[2], Joanna Nicholas[3], Xiang Zhang[2], Cui Er Seow[3]

[1] National Structural Integrity Research Centre, Cambridge, United Kingdom, CB21 6AL
[2] Coventry University, Coventry, United Kingdom, CV1 5FB
[3] TWI, Cambridge, United Kingdom, CB21 6AL

Abstract

Additive manufacturing (AM) techniques enable the production of near-net shape parts. Wire-arc direct energy deposition (WA-DED) can achieve a higher deposition rate among other available metal AM methods. Conventional arc welding requires a maximum interpass temperature to limit any reduction in mechanical properties, but this may not be practicable for wWA-DED. In this study, two interpass process control methods, one with maximum interpass surface temperature and the other with constant dwell time, were adopted to deposit low alloyed steel walls while maintaining the same feedstock and heat input values. Thermocouples were inserted at three different positions in the walls during deposition, to record the thermal profiles. Test samples extracted from walls exhibited similar tensile strength (~10 MPa difference) and hardness values. Microstructural evaluation showed the presence of interlayer regions with alternating coarse and fine bands of ferrite grains, irrespective of the interpass control method. These findings suggest that dwell time control is better for productivity.

Keywords: Wire-arc DED, Low alloyed steel, interpass surface temperature, interpass dwell time, thermo-couple measurement.

Introduction

Wire-Arc Direct Energy Deposition (WA-DED) is an emerging metal Additive Manufacturing (AM) method that possesses the potential to revolutionize the way large metal parts are produced. Like other AM methods, WA-DED introduces a pool of liquified metal from the wire feedstock by the electric arc that is deposited upon a substrate to fabricate a 3-dimensional component. In comparison with other metal AM processes, WA-DED has higher deposition rates (15 - 160g/min) [1], the ability to fabricate structural components with shorter lead time, and high material usage efficiency [1]. Compared to laser based and electron beam based AM methods, the arc imparts high heat input during deposition. Combining the high heat input with repetitive deposition subjects the component to multiple reheating cycles. This gives rise to complex thermal cycles across different parts of the build contributing towards anisotropy in mechanical properties and microstructure [2,3]. Hence, the WA-DED process efficiency and material performance (microstructure and properties) of the as-deposited material are directly influenced by processing parameters, control methods, and feedstock composition [1]. Thus, extensive research has been made to optimise the processing parameters such as current, voltage, torch travel speed, wire feed speed, contact tip to work distance (CTWD), torch angle [4-6], and attempts have been made to introduce process control methods such as maintaining a constant interpass surface temperature [7] and dwell time [8, 9].

Given the considerable research work pursued in optimizing these conditions, less work has been done on establishing a relationship between process parameters, control method (interpass surface temperature and dwell time control), resulting thermal cycle and its impact on material microstructure and mechanical properties. This interdependent relationship directly affects the microstructural evolution and mechanical properties in the as-deposited condition. Measurement of thermal profile during deposition makes it possible to establish this correlation. In this work, in-situ thermal measurements with K-type thermocouples have been carried out during wide wall deposition to understand the effect of process parameters on peak temperature and cooling rates. The influence on interpass control methods on the thermal profile is also done for the purpose of comparison.

Experimental methods

In the current study, two thick wall depositions of low carbon steel were fabricated by WA-DED system (as shown in Figure 1(a)), with in-situ temperature measurements made using K-type thermo-couples embedded within the wall during deposition. Two interpass process control methods were used for deposition of the walls, i.e., maintaining maximum (i) surface temperature (250°C) and (ii) dwell time (200s). Thermo-couples were placed at three different regions of the wall during deposition, for in-situ temperature measurements. The thermal history obtained includes local cooling rates experienced and peak temperature attained during subsequent reheating stages (i.e., next layers).

The chemical composition of the wire feedstock obtained from ESAB, is given in Table 1. The WA-DED system comprises a Fronius CMT advanced 4000R welding power source with a FANUC ARC Mate 120iC six-axis industrial robotic arm for housing and automated welding torch movement. The shielding gas used during the deposition process is M26 gas [10] along with an extraction unit. The heat input was set at a constant value of 2.4 kJ/mm by selecting the process parameters such as current (I), Voltage (V), travel speed (v) and wire feed speed (WFS) as given in Table 2. Heat input values were constantly recorded through the process using a AMV 4000 welding monitor (Triton Electronics Ltd, UK). For temperature measurement, calibrated K-type thermocouples of wire diameter 1mm, were used. The thermo-couples were ceramic insulated to guard from overheating by the electric arc during subsequent deposition. The overall time taken for depositing two walls were approximately 9 hours (for W1) and 7 hours (for W2), respectively. Different samples extracted for mechanical testing are specified in Table 3.

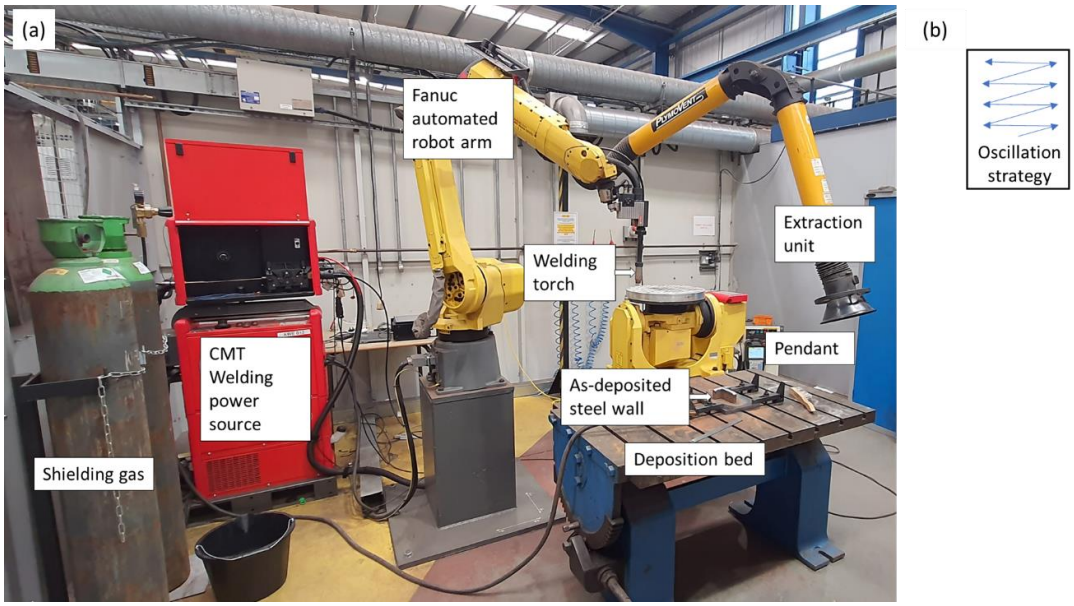

Figure 1: (a) Wire-Arc DED setup for low carbon steel wall deposition. (b) Deposition strategy for thick wall depositions.

Table 1: Chemical composition of ER70S-6 solid wire feedstock from ESAB (in wt%).

C	Si	Mn	Cr	S, P	Fe
0.08	0.5	1.5	0.02	<0.015	Balance

Table 2: Process parameters chosen for depositing two low carbon steel wall depositions.

Process parameter	Current (A)	Voltage (V)	Travel speed (mm/s)	Wire feed speed (m/min)	CTWD (mm)	Shielding gas flow rate (l/min)	Heat input (kJ/mm)
	204	20.6	1.95	8.4	15	16	2.406

Table 3: Summary of deposited walls and samples extracted in the as deposited condition.

WA-DED wall No.	Interpass control method	Temperature measurements	Test samples extracted
W1	Maximum 250°C surface temperature	M1, M2, M3	4 Tensile (horizontal) 4 Tensile (vertical) 10 Charpy (notch parallel) 10 Charpy (notch perpendicular)
W2	Maximum 200s dwell time	M1, M2	4 Tensile (horizontal) 4 Tensile (vertical) 10 Charpy (notch parallel) 10 Charpy (notch perpendicular)

Two S355 low carbon steel plates of dimensions 400 mm x 154 mm x 25 mm were used as substrates. The substrate surface was deburred with a steel wire brush and cleaned with acetone before the deposition. To obtain uniform heat distribution profile for a layer, oscillated or weave strategy was adopted where the welding torch travels across the width of the layer in an oscillating manner (as shown in Figure 1b).

A total of 59 layers were deposited to reach the wall height of 203 mm with thickness 26 mm and length 325 mm. The regions of thermocouple insertion (TC-M1 to TC-M3) are shown in Figure 2. After deposition, the walls were sectioned from the substrate and surface grinded to individual plates which were non-destructively tested with X-ray radiography to identify regions of macro-defects and thermo-couple insertion. Tensile, hardness and charpy impact test samples were extracted from the as-deposited walls as shown in Figure 2. The specimens were extracted across two different orientations, vertical (parallel to the build direction) and horizontal direction (perpendicular to the build direction).

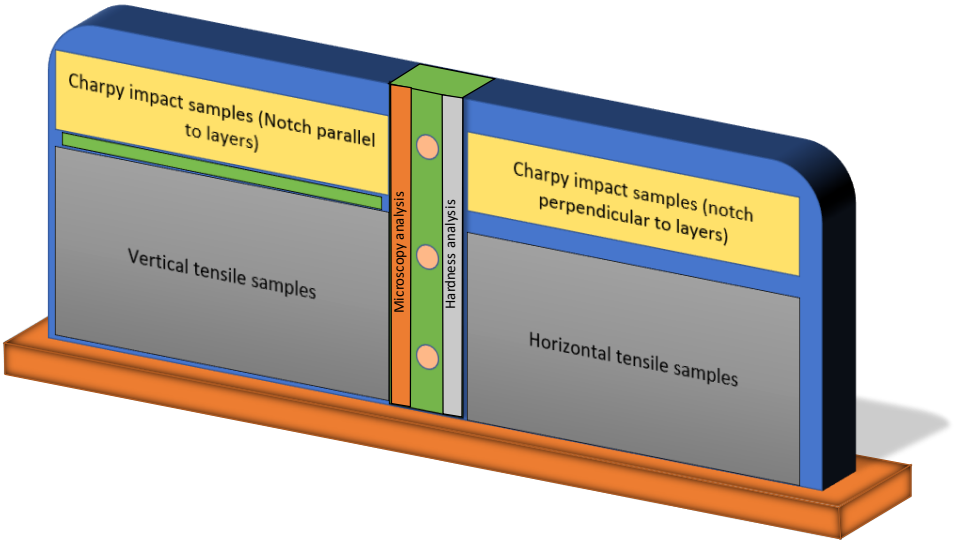

Figure 2: Specimen extraction plan for mechanical testing (tensile, hardness and Charpy) and microstructural analysis. M1, M2 and M3 denote the thermo-couple positions.

Results and Discussion

The in-situ measurements made by the thermo-couples placed at three different regions of the wall, M1 (top), M2 (mid), and M3 (bottom) are given in the Figure 3. The maximum range of the thermo-couple measurement is 1400°C which makes it difficult to measure the thermal cycle for the first pass, as the temperature under the arc reaches as high as 2600°C. Hence, temperature recording was resumed from the second pass of deposition, and the cooling rate values were calculated from passes that attain full austenisation during reheating.

Table 4: Summary of time taken to cool from 800C to 500C ($t_{8/5}$) and the cooling rates from regions M1-M3 for W1 and W2.

Sample	**W1**			**W2**	
	M1	**M2**	**M3**	**M1**	**M2**
$t_{8/5}$ (s)	58.7	60.8	64.2	110	90
Cooling rate (°C/s)	5.11	4.93	4.67	2.73	3.3

The thermal history experienced at different regions of deposition along with their corresponding cooling rates and $t_{8/5}$ is given in Figure 3 and Table 4 respectively. The thermal history from the bottom region of W2 is not included due to thermo-couple detachment from

the wall, after second pass of deposition, leaving with only one recorded pass of deposition. The cooling rates are calculated from the time taken for the layer to cool down from 800°C to 500°C, $t_{8/5}$, similar to calculations made for weld temperature measurements. The $t_{8/5}$ value for all measurements was calculated from the third deposition pass except for the middle region measurement of W2 (W2.M2) since it did not undergo full re-austenisation after the second deposition. In comparison, W2 had a slower cooling rate which is due to heat accumulation, also evident from the increasing interpass surface temperature (from Figure 3).

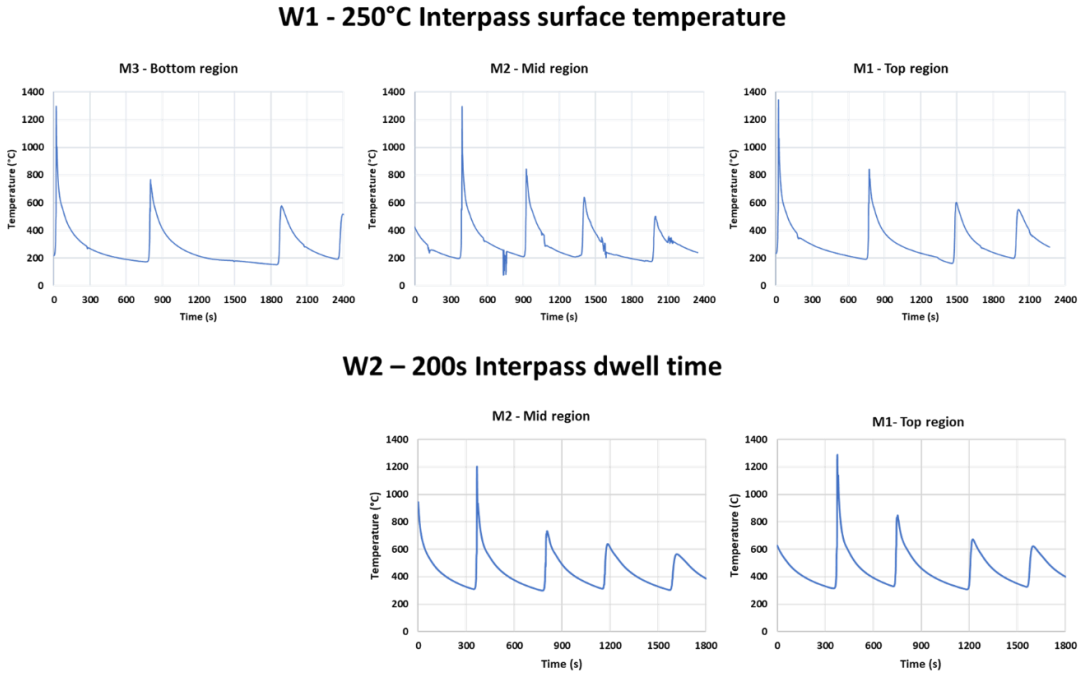

Figure 3: Temperature measurements from different regions of the as-deposited wall. M1 - Top region, M2 - Middle region and M3 - Bottom region

Microstructural analysis

Metallographic samples were extracted 3 cm away from the thermo-couple inserted region (M1-M3) to avoid any compositional change due to diffusion from thermo-couples. Since the samples are extracted closer to the thermocouples, they were considered to possess the sample thermal profile as M1-M3 regions and referred with the same nomenclature. The samples were mounted in Bakelite (as shown in Figure 4(a)), then grinded and polished with different silicon carbide polishing papers followed by polishing with 3µm, 1µm, and 0.25µm diamond suspensions. The preparation was finished by polishing with 40nm silica suspensions for optical microscopy and Electron Back Scattered Diffraction (EBSD) analysis. Initial analysis commenced with light optical microscopy, after which grain size determination was continued with EBSD analysis. Finally, the samples were tested for hardness values after microscopy analysis.

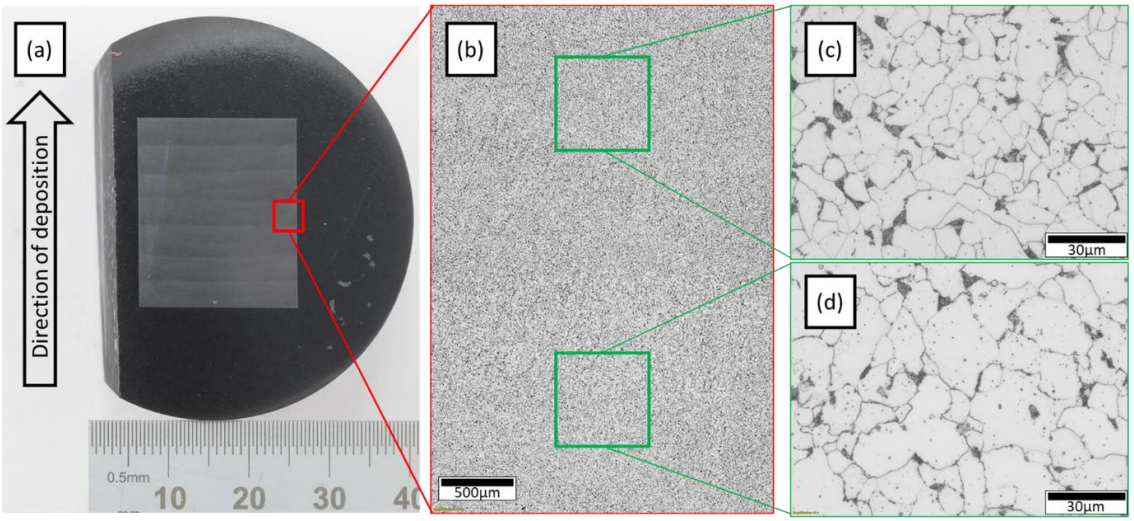

Figure 4: (a) W1 -Macrophotograph. (b)shows the interpass regions with alternating bands of coarse and fine ferrite grains. Optical micrographs of (c) fine grained and (d) coarse grained region

Upon etching with 2% Nital, it was observed from macro-photographs (Figure 4(a)), the presence of interlayer regions corresponding to layer height for each pass of deposition, for both the walls. The interlayer regions were present for both the walls, W1 and W2, across the deposition height. For the sake of reporting, one metallographic sample is chosen (W1.M1) and its microscopy results are shown in this section, while the quantitative results were obtained by performing the same analysis on all these samples. For W1.M1, the mounted and etched samples were viewed under optical microscope to reveal the presence of coarse and fine grained regions in the interlayers (Figure 4(b)). Upon viewing at higher magnification, the difference in grain size is evident, with regions of fine and coarse equiaxed ferrite grains, as shown in Figure 4(c) and Figure 4(d), respectively. For W1.M1, the Inverse Pole Figure (IPF) map is shown in Figure 5.

To quantify this difference in grain size and its distribution, further microstructural analysis was conducted with an Oxford Instruments NordlysMax EBSD detector fitted on a Zeiss Sigma Scanning Electron Microscope (SEM). The step size chosen for EBSD analysis was 1 µm while the grains were analysed with minimum detection area of 10 pixels (10 μm^2) and a critical misorientation of 5°. Since the width of these interlayer regions varied from 3 to 3.5mm, automated scans across the build direction were done to construct a montage area across the interlayer region. Again, to demonstrate the difference in grain size and distribution between these regions, sample W1.M1 is chosen for representation. From these scans, coarse and fine-grained regions were highlighted as different subsets, as shown in Figure 5, to estimate the average grain size and its distribution. The IPF map exhibits lack of any preferred crystallographic orientation in the microstructure, which is commonly reported from other AM processes [11] and wire-DED deposition of other alloys [12]. Lack of preferred orientation was observed from EBSD analysis of other samples too.

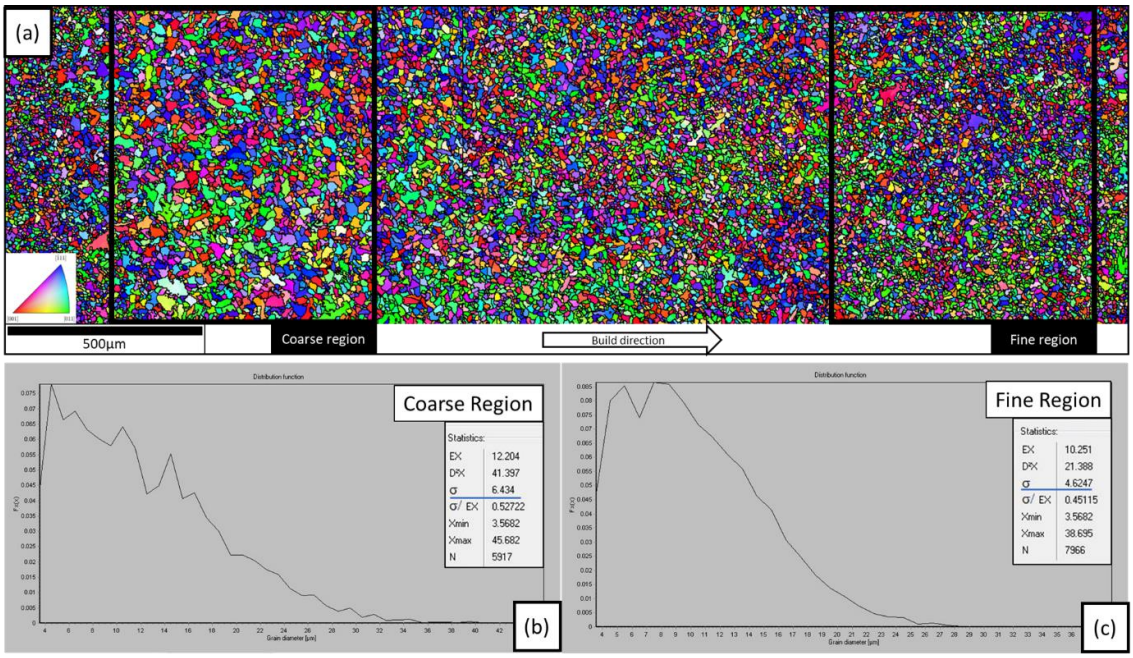

Figure 5: (a) EBSD Inverse Pole Figure (IPF) maps scanned across the interpass region of W1.M1 position to analyse the (b) coarse and (c) fine grain regions along with grain size distribution.

Determination of grain size and distribution were made according to the previously mentioned criteria. The average grain size measured from the coarse and fine-grained regions were 6.43µm and 4.62µm, respectively. Given the difference in average grain size is less significant, further EBSD analyses were analogously made across the interpass region and grain statistics were determined from the whole scan, instead of dividing the scanned region into different subsets (coarse and fine grained regions).

Rest of the microscopy samples were analysed by wide montaged EBSD scans to obtain more grain information (like W1.M1 analysis). The average grain size values and their distribution, for different microscopy samples, are given in Table 5 and Figure 6, respectively. Despite the difference in thermal profile and cooling rate (~3°C/s between W2 and W1) the grain size distribution remains similar across the deposition for W1, while for W2, as the deposition progresses slight coarsening is evident. This can be observed by the variation in grain size across build direction (i.e., M1 to M3) for W2.

Table 5: Average grain size determined from montaged EBSD scans for different metallographic samples.

Sample		**W1**	**W2**
Average grain size (µm)	**M1**	10.04 ± 5.3	11.26 ± 5.6
	M2	10.49 ± 5.8	12.24 ± 5.8
	M3	10.5 ± 5.7	10.5 ± 5.5

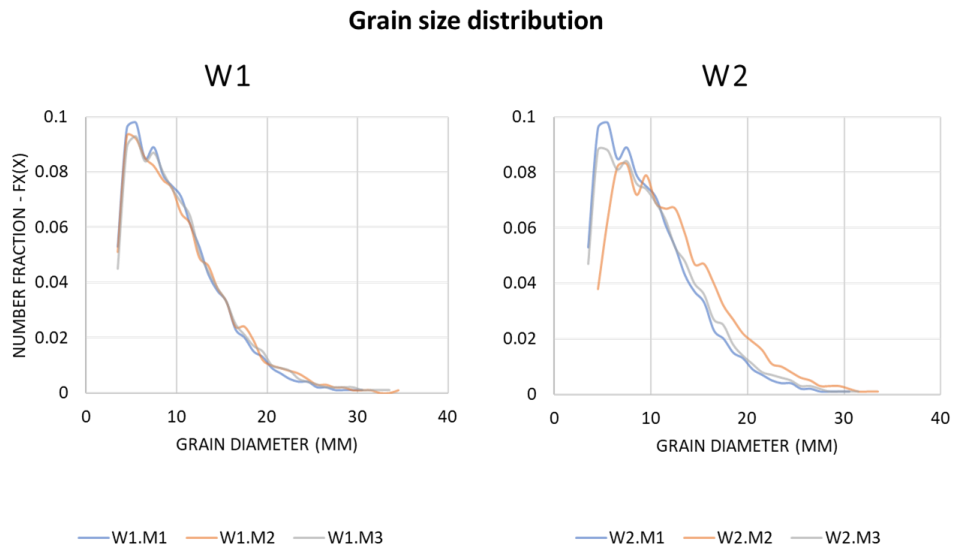

Figure 6: Average grain size distribution analysed from EBSD scans across different location (M1 - M3)

Following EBSD analysis, the prepared samples (extracted along the wall height, Figure 2) were tested for hardness and the measurement was done according to BS EN ISO 6507-1-2018 standard with a load of 5 kgf. The variation in hardness is shown in Figure 7. Three layers from the top and bottom of the walls were not measured as they were sectioned out before grinding the sample surface. As observed from the plot, the hardness varied between 140-160 HV and remained consistent along the deposition height, as reported in other thick wall depositions of low alloyed steels [13].

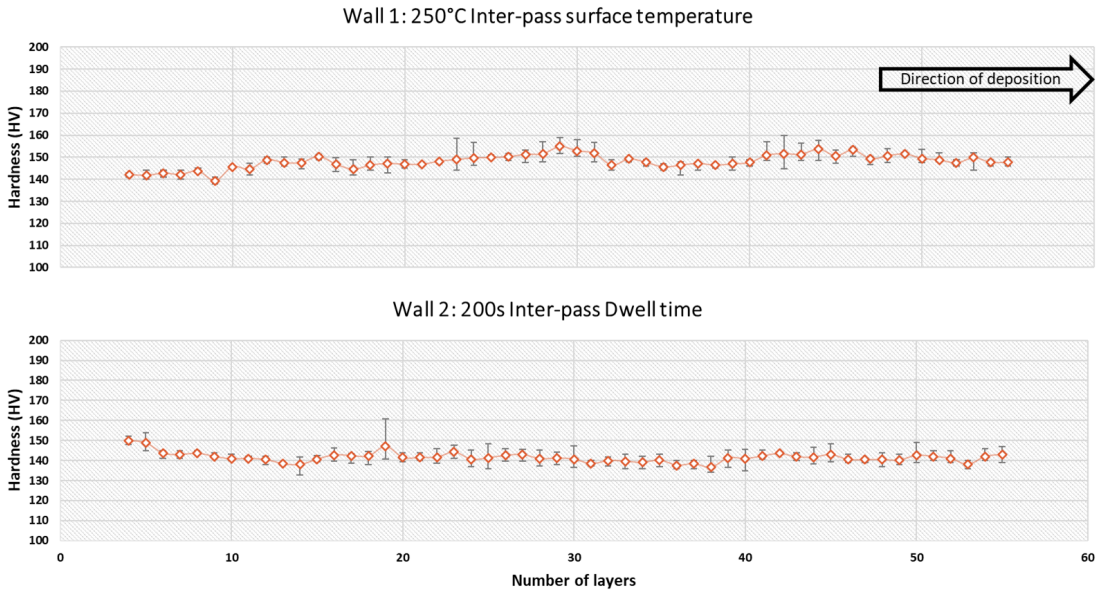

Figure 7: Variation of hardness along the deposition height.

Mechanical testing:

Tensile samples extracted from the wall shown in Figure 2, were tested according to the BS EN ISO 6892-1-2019 standard for two different material orientations.

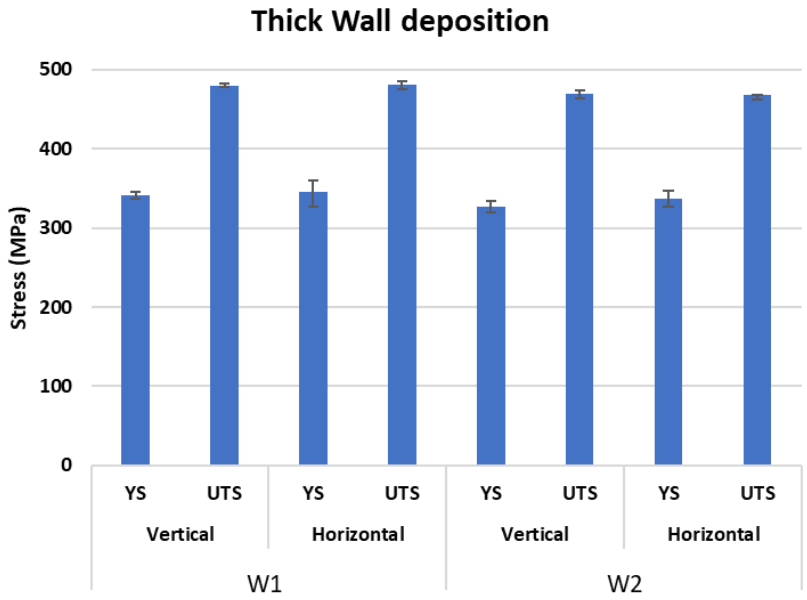

Figure 8: Yield and ultimate tensile strength values for W1 and W2 across two different orientations.

The tensile properties are shown in Figure 8. Irrespective of the control methods (interlayer temperature or dwell time) and material orientation, W1 and W2 had similar values of the ultimate tensile strength of 480MPa and 470MPa, respectively. The yield strength values were 345 MPa and 332 MPa for W1 and W2, respectively. This corresponds well with previous observations by testing samples extracted from WA-DED manufactured low alloyed steel walls [11, 12]. The lack of anisotropy in tensile properties can be due to the absence of preferred orientation (Figure 5) and the presence of equiaxed ferrite grains in the microstructure [13].

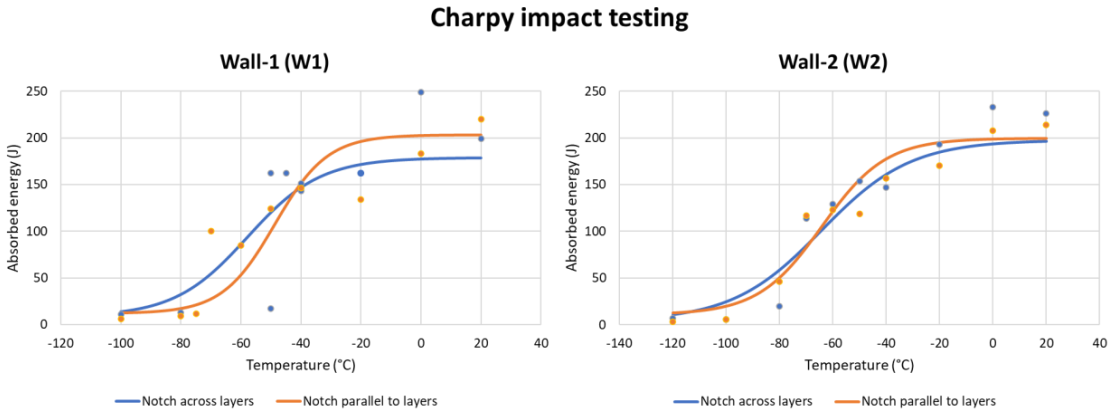

Figure 9: Charpy impact test result for samples extracted from Walls 1 and 2 in two different orientations, notch parallel or notch perpendicular to build direction, tested across the transition temperature range.

Charpy impact testing was conducted for standard-sized samples extracted from two different orientations, notch parallel or notch perpendicular to the build direction according to

the BS EN ISO 148-1-2010 standards. Prior to the impact testing, the samples to be tested in temperatures below the room temperature where immersed in methyl alcohol bath for 4 minutes at the target temperature. After attaining the test temperature, the samples were shifted to the testing chamber, where they were impact tested. Testing was done across a range of temperatures to determine the transition temperature and the temperature for different absorbed energies are given in Table 6.

Table 6: Transition temperature values (°C) for the corresponding absorbed energy values for the impact samples tested.

Sample	W1		W2	
	Horizontal (Notch perpendicular)	**Vertical (Notch parallel)**	**Horizontal (Notch perpendicular)**	**Vertical (Notch Parallel)**
$\mathbf{T_{27J}}$**(°C)**	-83.8	-70.3	-98.3	-92.6

For the samples tested at room temperature, the samples tested from W1 and W2 had absorbed energy values of ~200J. Comparing this result from literature on wire-arc DED depositions tested at room temperature, sub-sized specimens had lower impact energies [14] while regular sized samples had absorbed energy values of ~250J with observations of slight scatter in the toughness values [15, 16]. A wide scatter is observed for samples manufactured by the parallel deposition strategy [16], and it has been correlated with the microstructure being dependent on the phase formation. Rapid cooling after re-austenization led to Martensitic-Austenitic (MA) constituents which drastically influenced the scatter in impact toughness values, while slower cooling rate lead to fine pearlites formation enhancing the toughness values [16]. Overall, the impact toughness values are better for W2 on comparison with W1. The impact values demonstrate slight anisotropy, with notch perpendicular performing better than notch parallel samples for W1. In comparison, W2 has lower transition temperature values that are consistent across testing orientation. The impact properties obtained in this study display better result owing to the slower cooling rate during deposition (from Table 4) that leads to fine equiaxed microstructure with no preferred orientation (Figure 5 and Figure 6).

Conclusion

The microstructure and mechanical properties of WA-DED samples deposited using two interpass process control methods were characterised. On comparison, the two depositions have exhibited similar microstructural features, manifested by equiaxed ferrite grains without preferred grain orientation. The deposition made with interpass dwell time control displayed a slightly wider grain size variation than the deposition made with interpass temperature control. The mechanical properties (i.e., hardness, tensile strength and impact properties) of the two depositions were similar irrespective of the material orientation. However, slight anisotropy was observed in the Charpy impact transition temperature for both depositions, with lower transition temperature observed in the notch perpendicular direction. Furthermore, the deposition made with interpass dwell time control exhibited a lower overall (ie in both orientations) Charpy impact transition temperature. This suggest that using interpass dwell time control is as effective as interpass temperature control for low alloyed steel depositions through the WA-DED method. However, this could be exclusive for thick wall depositions made through low alloyed steels which does not undergo complex phase transformations other than austenite to ferrite and carbide transition on reheating. Adopting dwell time method could be

beneficial as it reduces the overall deposition time (~2 hours), thereby increasing process efficiency while eliminating the need for additional equipment for monitoring the surface temperature during the process.

Acknowledgements

This publication was made possible by the sponsorship and support of Lloyd's Register Foundation. Lloyd's Register Foundation helps to protect life and property by supporting engineering-related education, public engagement and the application of research. The work was enabled through, and undertaken at, the National Structural Integrity Research Centre (NSIRC), a postgraduate engineering facility for industry-led research into structural integrity established and managed by TWI through a network of both national and international Universities. The work was also supported by Coventry University.

Authors would like to acknowledge TWI Ltd and Armouers & Braisiers' Gauntlet trust for awarding a travel grant that aided with the travel arrangements for participation at the conference.

References

[1] Rodrigues, T., Duarte, V., Miranda, R., Santos, T., & Oliveira, J. (2019). Current status and perspectives on wire and arc additive manufacturing (WAAM). Materials, 12(7), 1121. https://doi.org/10.3390/ma12071121

[2] Ermakova, A., Mehmanparast, A., Ganguly, S., Razavi, J., & Berto, F. (2022). Fatigue crack growth behaviour of wire and arc additively manufactured ER70S-6 low carbon steel components. International Journal of Fracture, 235(1), 47-59.

[3] Nagasai, B., Malarvizhi, S., & Balasubramanian, V. (2021). Mechanical properties of wire arc additive manufactured carbon steel cylindrical component made by gas metal arc welding process. Journal of Mechanical Behaviour of Materials, 30(1), 188-198.

[4] Liberini, M., Astarita, A., Campatelli, G., Scippa, A., Montevecchi, F., Venturini, G., . . . Squillace, A. (2017). Selection of Optimal Process Parameters for Wire Arc Additive Manufacturing. Procedia CIRP, 62, 470-474.

[5] Prado-Cerqueira, J., Camacho, A., Diéguez, J., Rodríguez-Prieto, &., Aragón, A., Lorenzo-Martín, C., & Yanguas-Gil, &. (2018). Analysis of favorable process conditions for the manufacturing of thin-wall pieces of mild steel obtained by wire and arc additive manufacturing (WAAM). Materials, 11(8), 1449.

[6] Sun, L., Jiang, F., Huang, R., Yuan, D., Guo, C., & Wang, J. (2020). Anisotropic mechanical properties and deformation behavior of low-carbon high-strength steel component fabricated by wire and arc additive manufacturing. Materials Science & Engineering. A, Structural Materials : Properties, Microstructure and Processing, 787, 139514.

[7] Kozamernik, N., Bračun, D., & Klobčar, D. (2020). WAAM system with interpass temperature control and forced cooling for near-net-shape printing of small metal components. International Journal of Advanced Manufacturing Technology, 110(7-8), 1955-1968.

[8] Yang, D., Wang, G., & Zhang, G. (2017). Thermal analysis for single-pass multi-layer GMAW based additive manufacturing using infrared thermography. Journal of Materials Processing Technology, 244, 215-224.

[9] Montevecchi, F., Venturini, G., Grossi, N., Scippa, A., & Campatelli, G. (2018). Idle time selection for wire-arc additive manufacturing: A finite element-based technique. Additive Manufacturing, 21, 479-486.

[10] ISO 14175:2008. (2008). Retrieved from https://www.iso.org/standard/39569.html

[11] Haden, C., Zeng, G., Carter, F., Ruhl, C., Krick, B., & Harlow, D. (2017). Wire and arc additive manufactured steel: Tensile and wear properties. Additive Manufacturing, 16, 115-123.

[12] Aldalur, E., Veiga, F., Suárez, A., Bilbao, J., & Lamikiz, A. (2020). Analysis of the wall geometry with different strategies for high deposition wire arc additive manufacturing of mild steel. Metals (Basel), 10(7), 1-19.

[13] Panicker, S., Nagarajan, H., Tuominen, J., Patnamsetty, M., Coatanéa, E., & Haapala, K. (2022). Investigation of thermal influence on weld microstructure and mechanical properties in wire and arc additive manufacturing of steels. Materials Science & Engineering. A, Structural Materials : Properties, Microstructure and Processing, 853, 143690.

[14] Waqas, A., Xiansheng, Q., Jiangtao, X., Chaoran, Y., & Fan, L. (2018). Impact toughness of components made by GMAW based additive manufacturing. Procedia Structural Integrity, 13, 2065-2070.

[15] Shassere, B., Nycz, A., Noakes, M., Masuo, C., & Sridharan, N. (2019). Correlation of microstructure and mechanical properties of Metal Big Area Additive Manufacturing. Applied Sciences, 9(4), 787.

[16] Sridharan, N., Noakes, M., Nycz, A., Love, L., Dehoff, R., & Babu, S. (2018). On the toughness scatter in low alloy C-Mn steel samples fabricated using wire arc additive manufacturing. Materials Science & Engineering. A, Structural Materials : Properties, Microstructure and Processing, 713, 18-27.